Fluid Dynamics and Co-located Conferences
June 24-27, 2013, San Diego, CA
21st AIAA Computational Fluid Dynamics Conference

CrossMark
click for updates

Towards a Two-Equation Algebraic Structure-Based Model with Applications to Turbulent Separated Flows

Alejandro Campos*, Karthik Duraisamy†, and Gianluca Iaccarino‡
Stanford University, Stanford, CA, 94305, U.S.A.

A new variant of the Algebraic Structure-Based Model (ASBM) of Langer & Reynolds (2003) is developed and applied in Reynolds-averaged Navier-Stokes (RANS) simulations of turbulent separated flows. In the ASBM, additional information in the form of structure tensors, such as the dimensionality tensor, is used to determine the Reynolds-stress distribution. In this work, we have selected k-ϵ based transport equations to compute the turbulent kinetic energy and turbulence time scale at an adequate level of accuracy. These equations are supplemented with an elliptic relaxation approach to represent the wall blocking effects. Additionally, a new linear transformation approach – inspired by existing eddy realignment within the ASBM formulation – is introduced to account for redistribution effects and inhomogeneity encountered in near-wall flows. It is observed that a strong implicit coupling of the mean flow and turbulence equations is required to achieve fully-converged steady-state solutions. The new model is first used to simulate a fully developed periodic channel flow, for which it is shown to perform extremely well in predicting the turbulence stress anisotropy. When applied to flows involving mild and massive flow separation, improved behavior is observed when compared to linear eddy viscosity models, but further refinements of the model are required to capture the details of the recirculation zone predicted by high-fidelity turbulence simulations.

Downloaded by STANFORD UNIVERSITY on March 2, 2016 | http://arc.aiaa.org | DOI: 10.2514/6.2013-2719

Nomenclature

$\mathbf{r}$, r_i	Position vector
$\mathcal{R}_{ij}$	Two-point velocity correlation tensor
a_{ij}	Eddy-axis tensor
B_{ij}	Wall-blocking tensor
C_f	Skin-friction coefficient
C_p	Wall pressure coefficient
D_{ij}	Dimensionality tensor
d_{ij}	Dimensionality tensor non-dimensionalized by $2k$
k	Turbulent kinetic energy
L	Turbulent length scale
M_{ijkl}	Fourth-rank tensor for pressure-rate-of-strain
p_{ref}	Reference pressure
p_{wall}	Pressure at the bottom wall
r	Magnitude of position vector
R_{ij}	Reynolds stress tensor
r_{ij}	Reynolds stress tensor non-dimensionalized by $2k$
Re	Reynolds number
Re_τ	Friction Reynolds number
S_{ij}	Rate of strain tensor
u'	Velocity fluctuation, or turbulence intensity, in the streamwise direction

*Ph.D. Candidate, Department of Aeronautics & Astronautics.
†Assistant Professor (Consulting), Department of Aeronautics & Astronautics.
‡Associate Professor, Department of Mechanical Engineering.

Copyright © 2013 by the American Institute of Aeronautics and Astronautics, Inc. All rights reserved.

u_i' Fluctuating velocity vector, $u_i = \langle u_i \rangle + u_i'$
U_∞ Reference velocity
u_τ Friction velocity
u_i Velocity vector
v' Velocity fluctuation, or turbulence intensity, in the cross-streamwise direction
w' Velocity fluctuation, or turbulence intensity, in the spanwise direction
w_i' Fluctuating vorticity vector

Conventions

$(\cdot)^+$ Variable expressed in wall units
$\langle \cdot \rangle$ Reynolds averaged quantity
$| \cdot |$ Absolute value

Symbols

$\boldsymbol{\kappa},\ \kappa_i$ Wavenumber vector
χ Flattening parameter
δ Channel half height
δ_ν Viscous length scale
ϵ Dissipation of turbulent kinetic energy
ϵ_{ijk} Permutation tensor
γ Helical parameter
κ Magnitude of wavenumber vector
ν Kinematic viscosity
Ω Magnitude of the rate of rotation vector
Ω_i Rate of rotation vector
Ω_{ij} Rate of rotation tensor
Φ Wall-blocking parameter
ϕ Jettal parameter
Φ_{ij} Velocity-spectrum tensor
ψ_i' Vector stream function
τ Turbulent time scale
τ_w Wall shear stress

.

I. Introduction

Turbulent flow separation can have a significant effect on the performance of numerous engineering devices, such as aircraft wings, turbine blades, curved ducts and pipes, and streamlined obstacles, among others. Separation in steady two-dimensional flows over smooth surfaces occurs when a boundary layer subjected to an adverse pressure gradient over a streamwise distance reverses in flow direction or when a vanishing surface shearing stress occurs. An accurate prediction of such separated flows is a significant challenge for Reynolds-averaged Navier-Stokes (RANS) models. Predictions by a single RANS model for different separated flows are often inconsistent, which leads to low levels of confidence in such closure.

Multiple features of separate flows pose a challenge to the accuracy of a model. For separation from smooth surfaces, the separation process depends highly on the properties of the incoming boundary layer, such as the Reynolds stress anisotropy. Capturing such anisotropy thus becomes important. Moreover, there is a sharp increase in the turbulence energy and shear stress along the separation line.[1] Additionally, the state of the flow around this separation line has a strong effect on the characteristics of the separated shear layer, and a strong influence on the reattachment point.[2] Finally the flow may experience large-scale unsteadiness and is in a state far-off from turbulence equilibrium.

For smooth surfaces, the separation process is highly sensitive to the turbulent structures in the incoming boundary layer, such as near-wall streaks.[1] Moreover, the whole recirculation region within a separation bubble is dominated by large-scale energetic eddies with strong deformation and dynamics.[2] Structure-Based Models (SBMs), which focus on the statistical properties of structures, have the potential to simulate separated flows with a higher degree of accuracy.

Downloaded by STANFORD UNIVERSITY on March 2, 2016 | http://arc.aiaa.org | DOI: 10.2514/6.2013-2719

Downloaded by STANFORD UNIVERSITY on March 2, 2016 | http://arc.aiaa.org | DOI: 10.2514/6.2013-2719

Structure-based models attempt to describe the statistical properties of flow structures by providing a more complete characterization of the turbulent fluctuations. They do so by considering both the *componentality* and *dimensionality* of turbulence.[3,4] The componentality refers to the magnitudes of the three velocity fluctuations (u_1', u_2', u_3') along with magnitudes of their correlations, at a point in space. This property is thus quantified by the Reynolds stress tensor. The dimensionality, however, refers to the variations of these velocity fluctuations in all spatial directions, at a point in space, irrespective of the magnitude of such fluctuations. Kassinos & Reynolds [3] argue that in a one-point closure model, the anisotropy of a turbulent flow is not fully characterized by the anisotropy of the componentality alone, but also by the anisotropy of other physical properties, such as the dimensionality. These two properties, among others, can be used to describe localized structural characteristics of the flow.

The engineering outcome of structure-based modeling has been the Algebraic Structure-Based Model (ASBM). The first version of the ASBM was introduced by Haire,[5] who tested the model for homogeneous and free shear flows. Langer & Reynolds[6] improved the parametrization of the model used by Haire,[5] introduced the elliptic relaxation approach needed for wall-bounded flows, and formulated transport equations for k and ω^2 (enstrophy) needed to provide the time and length scales to the ASBM. The model was then tested for flat periodic channels, both in a fixed and rotating reference frame. Kassinos[7] coupled the ASBM with the v^2-f model of Durbin[8] and the k-ω model to obtain the time and length scales, instead of the k-ω^2 model of Langer & Reynolds, and used it to simulate periodic flat channel and flat-plate boundary layer flows. Radhakrishnan et al.[9] were the first to apply the ASBM to more complex flow phenomena, such as separated flows in a backward-facing step and an asymmetric diffuser. Their formulation of the ASBM was coupled with the v^2-f model. An examination of the parametrization of the model, with the goal of improving both accuracy and convergence, was conducted by Pecnik et al.[10]

In this paper we focus on both severe and shallow separated flows, which represent a significant challenge for all RANS models. Our focus has been on separation from smooth walls, thus introducing the need to predict the point of separation, as opposed to separation due to discontinuous surfaces examined by Radhakrishnan et al.[9] Based on considerations of accuracy, robustness, and simplicity, we have selected turbulent transport equations for the evolution of the turbulent kinetic energy and its dissipation to obtain the time and length scales required by the ASBM formulation.

The paper first provides a brief introduction to the structure tensors that are at the core of the ASBM. A description of the formulation of the ASBM, the required turbulent transport equations for the time and length scales, and a novel treatment of wall-blocking effects is then given. Finally, results are presented for fully developed turbulent flow in a flat channel and separated flows over a periodic hill and a converging-diverging channel.

II. One-point Structure Tensors

A mathematical description of both the componentality and dimensionality can be formulated using the fluctuating stream function, or vector potential ψ'.[3] This stream function is defined as follows,

$$u_i' = \epsilon_{ijk}\frac{\partial \psi_k'}{\partial x_j} \qquad \frac{\partial \psi_i'}{\partial x_i} = 0 \qquad \frac{\partial^2 \psi_i'}{\partial x_k \partial x_k} = -\omega_i' \tag{1}$$

where the last relationship follows from the first two. The one-point structure tensor for the componentality is then expressed as follows,

$$R_{ij} = \langle u_i' u_j' \rangle = \varepsilon_{ist}\varepsilon_{jpq}\left\langle \frac{\partial \psi_t'}{\partial x_s}\frac{\partial \psi_q'}{\partial x_p} \right\rangle \tag{2}$$

and the one-point structure tensor for the dimensionality is defined as follows,

$$D_{ij} = \left\langle \frac{\partial \psi_k'}{\partial x_i}\frac{\partial \psi_k'}{\partial x_j} \right\rangle. \tag{3}$$

It is important to note that while these tensors are defined at a point, they contain non-local information since the stream function, which satisfies a Poisson equation, is itself a non-local quantity. Additional structure tensors that contain further information about the flow can also be expressed in terms of the fluctuating stream function.[4]

The importance of the dimensionality tensor, and its relevance to the characterization of turbulence structures, will now be discussed. For homogeneous flows, Bhattacharya, Kassinos & Moser[11] derived expressions

for the only non-zero contractions of the fourth rank tensor M_{ijkl} used for modeling the pressure-rate-of-strain tensor. One contraction, as expected, is the Reynolds-stress tensor, whereas the other is the dimensionality tensor.

$$R_{ij} = M_{ijkk} = \int \frac{1}{|r|} \frac{\partial^2 \mathcal{R}_{ij}(\mathbf{r})}{\partial r_k \partial r_k} d\mathbf{r} = \int \Phi_{ij} \frac{\kappa_k \kappa_k}{\kappa^2} d\boldsymbol{\kappa} \tag{4}$$

$$D_{ij} = M_{kkij} = \int \frac{1}{|r|} \frac{\partial^2 \mathcal{R}_{kk}(\mathbf{r})}{\partial r_i \partial r_j} d\mathbf{r} = \int \Phi_{kk} \frac{\kappa_i \kappa_j}{\kappa^2} d\boldsymbol{\kappa} \tag{5}$$

Thus the information encapsulated in M_{ijkl} corresponding to the direction of the Fourier modes, which is not contained in the Reynolds stresses themselves, is contained in the dimensionality tensor. Bhattacharya, Kassinos & Moser[11] then show that for certain anisotropic forms of the two-point correlation, this anisotropy is captured *entirely* by the dimensionality tensor whereas the associated Reynolds-stress tensor assumes an isotropic form. It is thus clear that both R_{ij} and D_{ij} are independent properties that influence the evolution of the turbulence, through the M_{ijkl} tensor and the corresponding pressure-rate-of-strain term (see also Mansour, Shih & Reynolds ;[12] Kida & Hunt ;[13] Cambon, Jacquin, & Lubrano[14]).

The Reynolds-stress and dimensionality tensors, along with other one-point tensors defined by Kassinos, Reynolds & Rogers,[4] can be used to describe the physical properties of the turbulence structures. One can picture turbulence structures as having directions of independence, along which gradients of the velocity fluctuations are small, and directions of dependence, along which gradients of the fluctuations are large, in a statistical sense. The dimensionality tensor identifies these directions of dependence and independence since it represents gradients of the fluctuations exactly for homogeneous flows and with reasonable accuracy for inhomogeneous flows. For example, if $D_{11} = 0$,

$$\frac{\partial \psi_i'}{\partial x_1} = 0 \qquad \text{for } i = 1, 2, 3. \tag{6}$$

Since gradients of the fluctuations can be expressed as follows,

$$\frac{\partial u_i'}{\partial x_1} = \frac{\partial}{\partial x_1}\left(\epsilon_{ijk} \frac{\partial \psi_k'}{\partial x_j}\right) = \epsilon_{ijk} \frac{\partial}{\partial x_j}\left(\frac{\partial \psi_k'}{\partial x_1}\right) \qquad \text{for } i = 1, 2, 3 \tag{7}$$

the gradient of the velocity fluctuations in the x_1 direction is identically zero for homogeneous flows. The ability of the structure tensors to describe turbulence structures was showcased for a variety of homogeneous and inhomogeneous flows.[4] For example, close to the no-slip wall of a flat channel, $D_{11} \approx 0$ and $D_{11} \ll D_{22}, D_{33}$, which is in agreement with the streaky structures observed in numerous experiments and simulations.

III. Description of the Algebraic Structure-Based Model

The inputs required by the ASBM are the rate of strain and rotation tensors (normalized by the turbulent time scale) and a wall blocking tensor B_{ij} (obtained using an elliptic relaxation approach as detailed towards the end of this section) that accounts for near-wall effects. A set of constitutive relations and parameterizations use such inputs to compute the non-dimensionalized structure tensors of Kassinos et al.,[4] which include the Reynolds stresses. The Reynolds-stresses are then dimensionalized using the turbulent kinetic energy and are then used to compute the viscous fluxes. The turbulent time scale along with the kinetic energy are thus required when using the ASBM, and these have typically been obtained using traditional Eddy-Viscosity Models (EVMs). A schematic of the integration of the ASBM with a CFD solver is shown in Fig. 1.

III.A. Constitutive relation, eddy-axis tensor, and structure scalars

In the ASBM formulation a set of intermediate tensors and parameters are computed with the goal of obtaining the final output, namely, the structure tensors. Such computations are based on the assumption that a general 3-dimensional, 3-component flow is composed of a superposition of hypothetical 2-dimensional, 3-component eddies.[3] These are eddies with one axis of independence – along which the dimensionality is zero – and two axes of dependence perpendicular to the first axis. Jetal turbulence refers to non-zero velocity fluctuations along the axis of independence. Vortical turbulence refers to non-zero fluctuations

Downloaded by STANFORD UNIVERSITY on March 2, 2016 | http://arc.aiaa.org | DOI: 10.2514/6.2013-2719

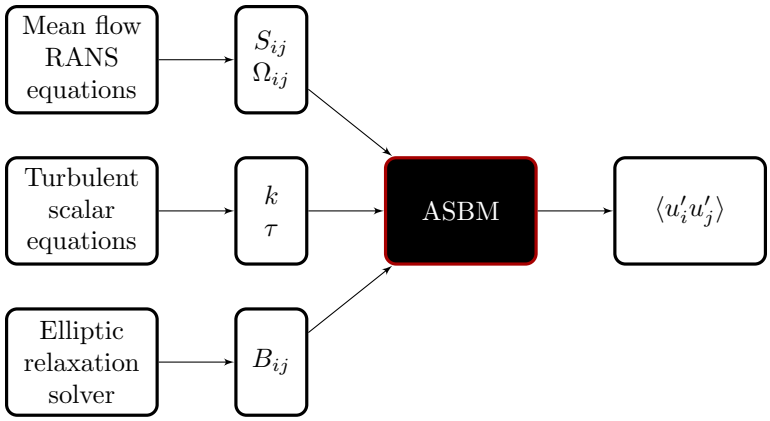

Figure 1. Schematic representation of the ASBM

Downloaded by STANFORD UNIVERSITY on March 2, 2016 | http://arc.aiaa.org | DOI: 10.2514/6.2013-2719

perpendicular to the axis of independence. Such eddy behaviors are quantified by the eddy-axis tensor a_{ij}, and three structure scalars: the jetal parameter ϕ, the helical parameter γ, and the flattening paramter χ. A spatial averaging procedure that allows one to obtain constitutive equations expressing the structure tensors in terms of the eddy axis tensor is used. Those constitutive equations follow,

$$\begin{aligned} r_{ij} = {} & (1-\phi)\frac{1}{2}(\delta_{ij} - a_{ij}) + \phi a_{ij} - \gamma \frac{1}{2}\frac{\Omega_r}{\Omega}(\epsilon_{ipr}a_{pj} + \epsilon_{jpr}a_{pi}) \\ & + \chi \left\{ (1-\phi)\left[\frac{1}{2}(1 - a_{nm}b_{mn})\delta_{ij} - \frac{1}{2}(1 + a_{nm}b_{mn})a_{ij} - b_{ij} + a_{in}b_{nj} + a_{jn}b_{ni}\right] \right. \\ & \left. - \gamma \frac{\Omega_k}{\Omega}(\epsilon_{ipr}a_{pj} + \epsilon_{jpr}a_{pi})\left[-\frac{1}{2}(1 - a_{nm}b_{mn})\delta_{kr} + b_{kr} - a_{kn}b_{nr}\right]\right\} \end{aligned} \tag{8}$$

$$d_{ij} = \frac{1}{2}(\delta_{ij} - a_{ij}) + \chi\left[-\frac{1}{2}(1 - a_{nm}b_{mn})\delta_{ij} + \frac{1}{2}(1 + a_{nm}b_{mn})a_{ij} + b_{ij} - (a_{in}b_{nj} + a_{jn}b_{ni})\right] \tag{9}$$

where,

$$b_{ij} = \frac{\Omega_i \Omega_j}{\Omega_k \Omega_k} \tag{10}$$

for fixed-frame rotations.

The eddy-axis tensor a_{ij} determines the axis of independence of the aforementioned hypothetical eddies.[3] For example, if $a_{11} = 1$ whereas all other components are zero, the axis of independence is mostly aligned with the x_1 direction. The computation of a_{ij} is performed in two steps: First, a_{ij} is computed assuming irrotational flow using an implicit algebraic equation that depends solely on the non-dimensional rate-of-strain tensor. A rotational correction corresponding to a matrix orthogonal transformation is then applied to kinematically adjust a_{ij} due to the mean-flow rotation.

The jetal parameter ϕ partially describes the componentality of the eddy. ϕ ranges from 1, which corresponds to purely jetal motion, to 0, which corresponds to purely vortical motion. The helical parameter γ provides additional information on the componentality of the flow, with a value of zero corresponding to either purely jetal or purely vortical motion, and non-zero values corresponding to a combination of both jetal and vortical motion. The hypothetical eddies were initially constructed assuming an axisymmetrical distribution for the dimensionality perpendicular to the axis of independence.[3] The flattening scalar χ was later introduced to represent the deviation from axisymmetry.[6]

The functions that define the three scalars ϕ, γ, and χ are obtained from a parametrization based on different states of turbulence. As described in Langer & Reynolds,[6] theoretical values for r_{ij} and d_{ij} are known for two limiting states, which are isotropic turbulence and rapidly distorted turbulence subjected to specific deformations, such as pure shear, plane strain, or a combination of both. Thus one can find the values for ϕ, γ, and χ that, when used in equations (8) and (9), provide structure tensors that are

in agreement with the theoretical values of isotropic turbulence and RDT. Interpolating functions are then used to obtain the functional form for the structure scalars away from such limiting states.

Overall, the ASBM formulation can be summarized as shown in Fig. 2. The inputs to the ASBM are the mean flow properties, such as S_{ij} and τ. Equations (8) and (9) are used in the final step to compute the structure tensors. It is important to note that these structure tensors were obtained based on a homogeneous analysis of the flow, and inhomogeneities are accounted for using the blocking tensor B_{ij}, as described in the following section III.B.

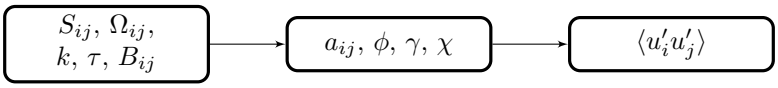

Figure 2. Inside the ASBM black box.

III.B. Near wall treatment

As described thus far, the ASBM essentially predicts structure functions and Reynolds stresses corresponding to quasi-homogeneous states of turbulence. Near a solid wall, however, it is well recognized that the blocking effect introduced by the impenetrability constraint suppresses the wall-normal velocity fluctuations and introduces additional turbulence anisotropy by redistributing the energy of the turbulent fluctuations. The near-wall treatment in the present work is loosely based on the concept of elliptic relaxation of Durbin[15] to introduce a wall blocking tensor B_{ij}. A blocking parameter Φ is defined to be the solution of the following equation

$$L^2 \nabla^2 \Phi = \Phi, \tag{11}$$

with $\Phi = 1$ at the wall and $\partial\Phi/\partial x_n = 0$ at other boundaries, where n is the wall-normal direction. Note that the above equation is of the form $(1 - L^2\nabla^2)f = f_h$ as suggested by Durbin, with f_h representing the homogeneous value of the quantity of interest. The length scale L is defined as in Ref. 16,

$$L = C_L \max\left[\frac{k^{3/2}}{\epsilon}, C_\nu \left(\frac{\nu^3}{\epsilon}\right)^{1/4}\right], \tag{12}$$

where $C_L = 0.23$ and $C_\nu = 70.0$. The blockage tensor is finally defined as

$$B_{ij} = \frac{\frac{\partial\Phi}{\partial x_i}\frac{\partial\Phi}{\partial x_j}}{\frac{\partial\Phi}{\partial x_k}\frac{\partial\Phi}{\partial x_k}}\Phi. \tag{13}$$

The above definition is regularized by averaging over neighboring points when the denominator approaches zero. Prior versions of the ASBM[5,6] have attempted to use B_{ij} to re-align the eddy axis tensor such that the eddies near the wall are jetal in nature. An additional constitutive relationship was then used to recover the Reynolds stress tensor r_{ij}. In the present work, the blocking operation is performed directly on the quasi-homogeneous Reynolds stresses r^h_{ij} in terms of a partial projection operator[6] H_{ij} which is defined as

$$H_{ij} = \frac{\delta_{ij} - B_{ij}}{D_r}, \tag{14}$$

where,

$$D_r^2 = 1 - (2 - B_{kk}) r^h_{mn} B_{mn}. \tag{15}$$

A sequence of these operators are applied to the quasi-homogeneous Reynolds-stress tensor to obtain the wall-blocked version,

$$r_{ij} = H_{ik} H_{jl} r^h_{kl}. \tag{16}$$

As explained in Ref. 17, this projection operator results in a $O(y^2)$ and $O(y)$ behavior for r_{22} and r_{12}, respectively as $y \to 0$ when $B_{22} = 1 - O(y)$. For a fully developed channel flow, with x_2 the wall-normal direction, the wall blocking operation simplifies to $r_{11} = H_{11}^2 r^h_{11}$, $r_{22} = H_{22}^2 r^h_{22}$, $r_{33} = H_{33}^2 r^h_{33}$, and $r_{12} = H_{11} H_{22} r^h_{12}$. For illustrative purposes, these functions are shown in Fig. 3. A slight amplification of the streamwise fluctuations and significant reduction of the wall-normal fluctuations can be observed. It has to

Downloaded by STANFORD UNIVERSITY on March 2, 2016 | http://arc.aiaa.org | DOI: 10.2514/6.2013-2719

be recognized that the ASBM predicts significant anisotropy of the stresses even before the application of the wall-blocking operation. The effect of the wall-blocking operation on the Reynolds stresses themselves is shown in Fig. 4, which shows that the stresses follow the supposed asymptotic limits close to the no-slip wall when subjected to the above blocking procedure.

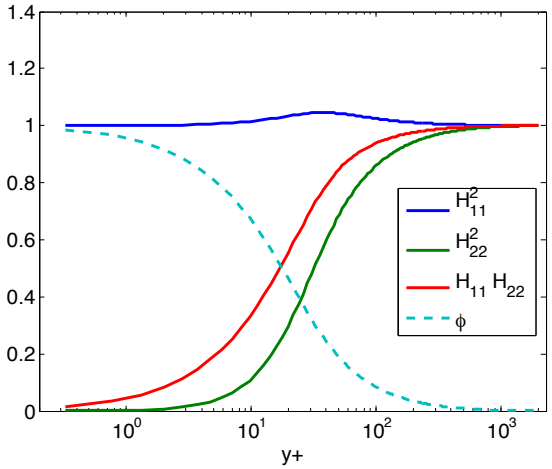

Figure 3. Wall blocking functions for a fully developed periodic channel, with x_2 the wall-normal direction, at $Re_\tau = 2003$.

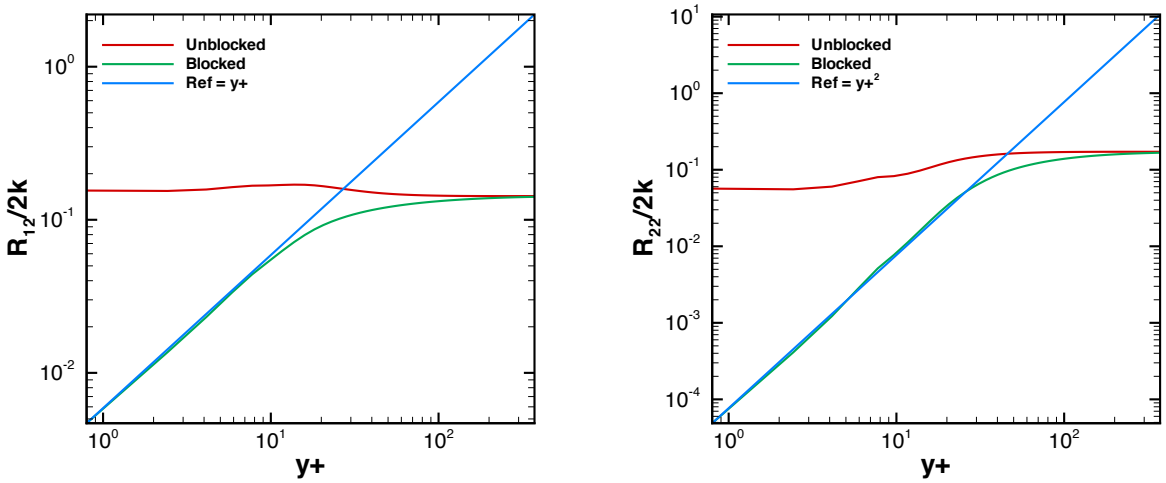

Figure 4. Profiles for shear and wall-normal stress components in a fully developed channel, with and without the application of blocking operators.

III.C. Turbulent scalar equations

The turbulent time scale, length scale and kinetic energy required by the ASBM are obtained from two turbulent scalars for which transport equations have to be solved. There are multiple candidates for these transport equations, corresponding to different EVMs in the literature. The transport equations of the SST model are likely candidates due to the favorable capabilities of the SST when compared to most linear EVMs, especially when predicting levels of shear stress. Our focus, however, is instead on the accuracy of the turbulence scalars themselves. Thus the SST model is not the optimal candidate since the near-wall behavior of the predicted turbulent kinetic energy is typically inferior to that of k-ϵ based models.

Downloaded by STANFORD UNIVERSITY on March 2, 2016 | http://arc.aiaa.org | DOI: 10.2514/6.2013-2719

We then shifted our attention to k-ϵ based models to provide the required turbulent scalars. Among this class, the v^2-f of Durbin[15] has been shown to predict some cases of separated flows with highest accuracy. We thus coupled the ASBM with the k and ϵ equations of the v^2-f model, but used the normal stress perpendicular to a streamline obtained from the ASBM to replace the velocity scalar v^2. One of the benefits of such a simplification is the reduction in computational cost obtained by reducing the number of transport equations from four to two, since the v^2 transport equation and the elliptic f equation required for the production of v^2 are unnecessary. Additionally, the wall-blocking effect is now characterized by a single parameter Φ, instead of both Φ and f, which leads to a redundant and incoherent approach. Another benefit is that the numerical instability of the v^2-f, due in part to the equations for v^2 and f, is ameliorated. This setup for the model, hereafter referred to as just the ASBM, was used for the simulations described in the results section.

Profiles of the turbulent kinetic energy in a fully developed flat channel flow obtained with the original EVMs and the ASBM coupled with the SST and the v^2-f, as described above, are shown in Fig. 5. The poor prediction of the turbulent kinetic energy by the SST and thus the ASBM coupled with the SST is apparent. The v^2-f model shows the turbulent kinetic energy in good agreement with DNS. The intensity of the turbulent kinetic energy is underpredicted by the ASBM coupled with the v^2-f model. The shape of this profile, however, more closely resembles that of the DNS, when compared to the v^2-f.

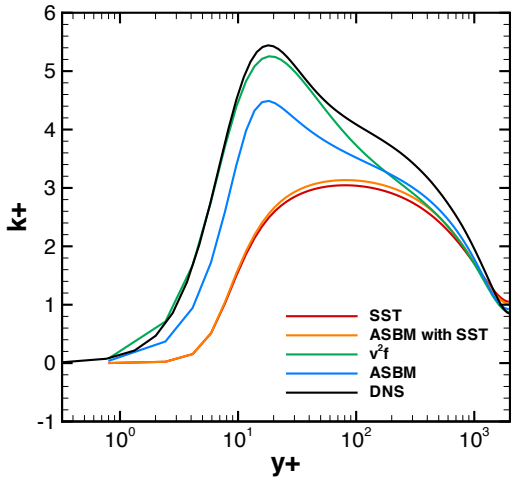

Figure 5. Profiles of the turbulent kinetic energy (in wall units) for a flat channel at $Re_\tau = 2003$.

IV. Numerical Method

The compressible Reynolds-Averaged Navier–Stokes equations are discretized using a cell-centered finite volume scheme on polyhedral unstructured meshes using the JOE solver.[18,19] A spatially second order accurate discretization is used for the convective and diffusive fluxes. Convergence to steady-state is achieved by pseudo time-stepping based on implicit Euler time integration. For the solution of the ASBM model, the linearized Jacobian at every outer flow iteration is constructed in a fully coupled manner, *i.e.* the mean flow (mass, momentum, energy) and k, ϵ equations are treated simultaneously. Such a strong coupling was found to be *essential* to achieve convergence for the ASBM model (as observed from Fig. 6) as a consequence of the extreme stiffness introduced by the absence of explicit near-wall damping functions in the k and ϵ equations. The resulting system of equations is solved using GMRES with ILU preconditioning.[20] In addition to the mean flow and turbulence scalar equations, an elliptic equation for the wall blocking function (ϕ, as defined in the previous section) is solved in an isolated fashion. Experimentation of supplementing the ASBM model with several choices of the turbulent scalar equations ($k-\epsilon$, v^2-f and $k-\omega$) was performed and inconsistent convergence behavior was observed. For the examples shown in the results section, the $k-\omega$ scalar set was identified to be the only model to exhibit good convergence properties without the use of the strong coupling.

Downloaded by STANFORD UNIVERSITY on March 2, 2016 | http://arc.aiaa.org | DOI: 10.2514/6.2013-2719

It is thus clear that the near-wall behavior and the synchronization between blocking tensor and damping appears to be of critical importance to achieve convergence in ASBM formulations.

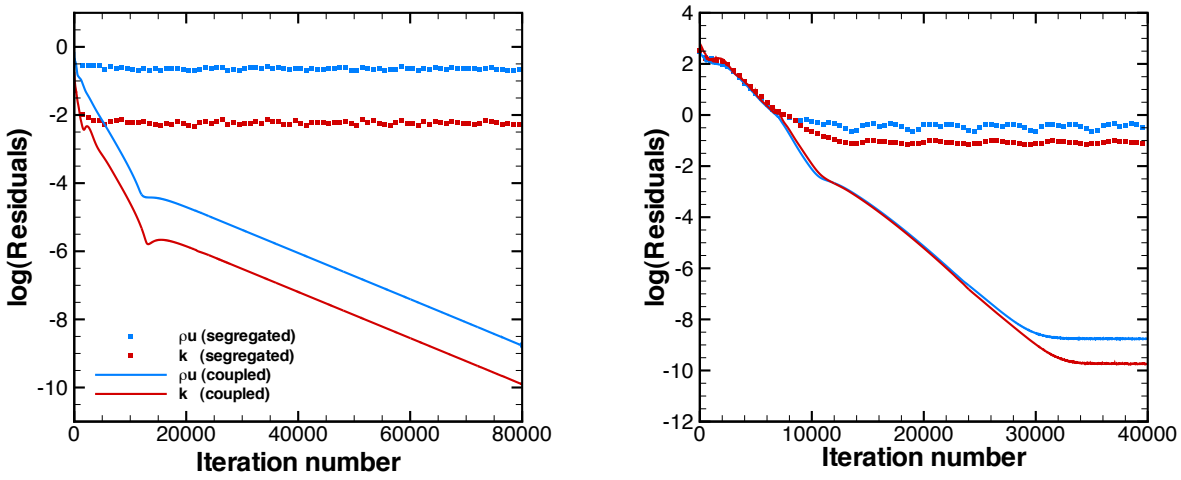

(a) Periodic Hill

(b) Converging-Diverging Channel

Figure 6. Convergence of mean streamwise momentum and turbulent kinetic energy for separated flows (described in Section V), using fully coupled and segregated methods of solution.

V. Results

V.A. Periodic Channel

Simulations of fully developed turbulent flow in two flat channels with different Reynolds numbers were used as first test cases to investigate the accuracy and numerical properties of the ASBM. The friction Reynolds number Re_τ, based on the friction velocity u_τ and channel half height δ, is equal to 395 for the first case and 2003 for the second case. These conditions correspond to the highly resolved direct numerical simulations conducted by Moser, Kim & Mansour[21] and Hoyas & Jimenez,[22] respectively. The high Reynolds number of the latter DNS allows us to investigate how well the ASBM can reproduce the high-Reynolds-number effects of a boundary layer, such as an appreciable log layer.

The channel mesh used for the RANS simulations has a height of $\delta = 1$, contains only four finite volumes in the streamwise direction, and uses periodic inlet and outlet boundaries. The flow is driven by a uniform streamwise body force applied over the entire domain, the value of which fixes the magnitude of the friction velocity.

The velocities normalized by the friction velocity are plotted as a function of wall distance in Fig. 7(a) and Fig. 7(b). The distance to the wall has been normalized by the viscous length scale $\delta_\nu = \nu/u_\tau$. Figure 7(a) shows that the velocity is slightly overpredicted by the v^2-f, k-ϵ, and ASBM models over the log law region and at the freestream location, whereas it is underpredicted by the SST model. The ASBM, however, predicts the free stream velocity magnitude closest to that of the DNS, with an error of 1.55%, and is then followed by the SST with an error of 2.45%. The ASBM predicts a slope for the velocity profiles in the log-law region that is closest in value to that of the DNS, whereas the EVMs tend to overpredict the slope of these profiles. All models correctly capture the behavior in the viscous sublayer.

Improved agreement for all models is observed for the higher Reynolds number case, as shown in Fig. 7(b). The freestream velocity is now accurately captured by all RANS models, with the ASBM error being 0.07%. The velocity profile of the ASBM exactly matches the log law profile in the range $y^+ = 30 - 300$ and is thus in good agreement with the DNS. The velocity profiles predicted by k-ϵ and v^2-f are also in high agreement with DNS. The SST model, however, predicts a slope for the velocity profiles that is slightly higher than that of the other models. As with the lower Reynolds number case, the viscous sublayer is accurately represented.

Profiles for the turbulence intensities and shear stress are shown in Fig. 8(a) and Fig. 8(b) for the low

Downloaded by STANFORD UNIVERSITY on March 2, 2016 | http://arc.aiaa.org | DOI: 10.2514/6.2013-2719

Downloaded by STANFORD UNIVERSITY on March 2, 2016 | http://arc.aiaa.org | DOI: 10.2514/6.2013-2719

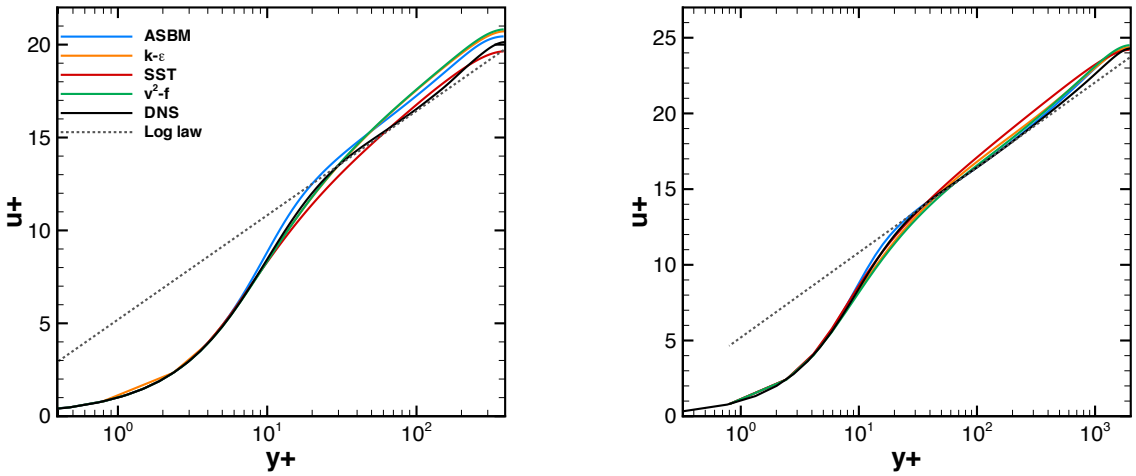

Figure 7. Streamwise velocity (in wall units) for fully developed periodic channels. (a) $Re_\tau = 395$**, (b)** $Re_\tau = 2003$**. For log law** $\kappa = 0.41$, $B = 5.2$.

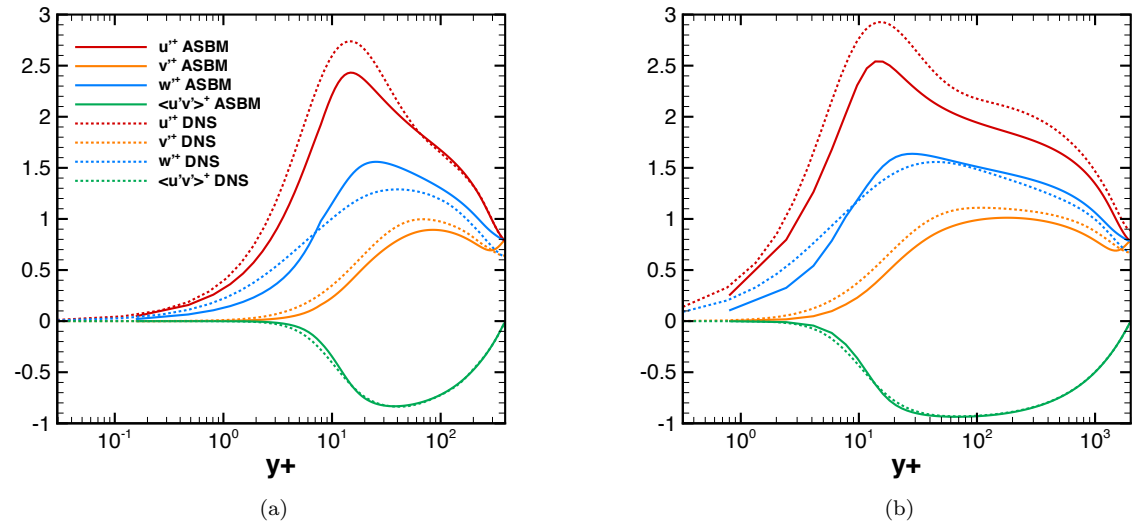

Figure 8. Turbulence intensities and shear stress normalized by the friction velocity for a periodic channel. (a) $Re_\tau = 395$**, (b)** $Re_\tau = 2003$.

and high Reynolds number cases, respectively. Most EVMs capture the shear stress accurately, but do not capture the anisotropy characterized by differences in the normal stresses. The ASBM, however, shows satisfactory agreement with the DNS data in the prediction of the normal stresses, for both cases. The freestream value of the streamwise turbulence intensity predicted by the ASBM is in agreement with the DNS, though the peak of the turbulence intensity is below the maximum of the DNS. The cross-streamwise intensity of the ASBM has the right shape, and is slightly underpredicted throughout the channel. The spanwise turbulence intensity of the ASBM shows larger curvature than that of the DNS, but improved agreement is observed for the higher Re_τ case. The ASBM shows all normal stresses to be of the same value at the channel half height, whereas some departure from an isotropic state is shown by the DNS. The shear stresses of the ASBM are in strong agreement with those of the DNS for both Reynolds numbers.

V.B. Periodic Hill

The LES of a periodic hill performed by Frohlich et al.[2] is a benchmark case used to test the quality of a model when used to simulate massively separated regions (e.g Jang et al.[23]). The domain consists of streamwise periodic hills on the bottom no-slip wall of a channel, and a straight no-slip upper wall. Periodic boundary conditions are applied in both the streamwise (x) and spanwise (z) directions to enforce fully two dimensional flow. The inter-hill distance is $L_x = 9h$, where h is the height of the hill. The height of the domain is $L_y = 3.035h$ and the span is $L_z = 4.5h$. Though the spanwise extent could be increased to allow for a full representation of the spanwise structures, Frohlich et al. state that the error introduced is small for the first- and second-order moments. The Reynolds number of the simulation, based on the bulk velocity at the peak of the hill and the hill height, is equal to 10595.

The RANS simulations used a mesh with the same geometry as that of the LES. The mesh lines depart the curved bottom wall orthogonally to aid convergence. A total of 30600 cells were used in the RANS mesh as opposed to 4.6 million cells used in the LES mesh. The $y+$ at the bottom wall ranges from 0.07 to 2.0, and has an average value of 0.58. Convergence of more than ten orders of magnitude of residuals was achieved using this grid and the ASBM model. Periodic boundary conditions were also enforced by the RANS simulations in the streamwise direction. The flow in our simulations was driven by a uniform body force chosen to match the same bulk velocity at the crest of the hill, and hence the Reynolds number.

Downloaded by STANFORD UNIVERSITY on March 2, 2016 | http://arc.aiaa.org | DOI: 10.2514/6.2013-2719

Downloaded by STANFORD UNIVERSITY on March 2, 2016 | http://arc.aiaa.org | DOI: 10.2514/6.2013-2719

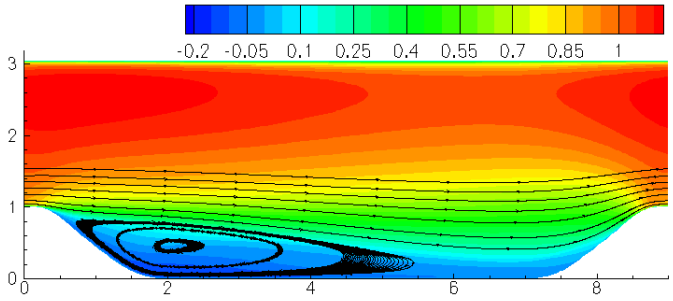

(a)

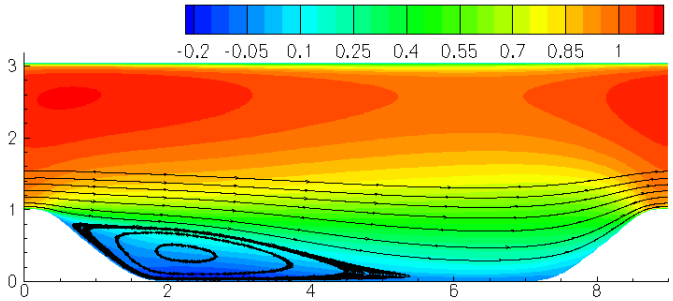

(b)

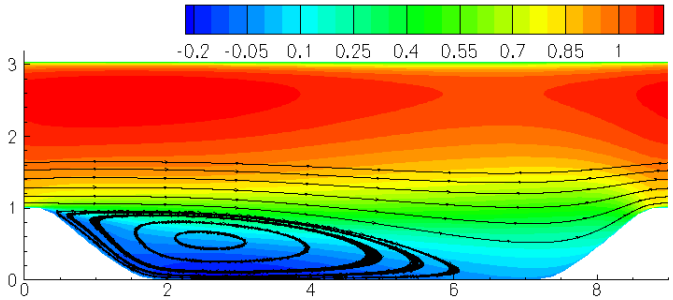

(c)

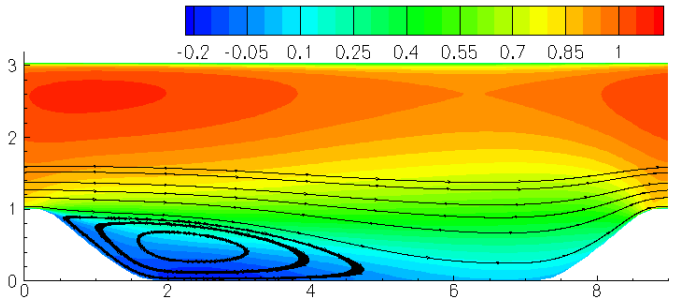

(d)

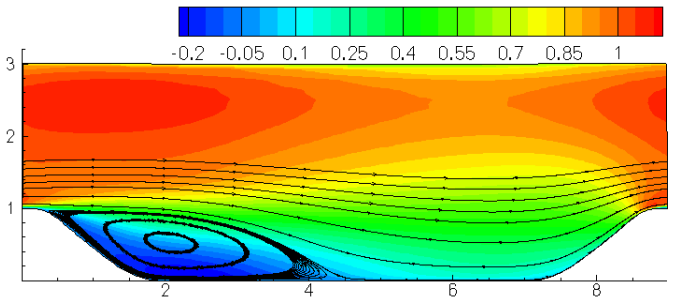

(e)

Figure 9. Velocity contours. (a) ASBM, (b) alternate ASBM, (c) SST, (d) v^2-f, (e) LES.

An overall view of the flow is shown in Fig. 9, which shows streamwise velocity contours along with streamlines close to the separation region. In Fig. 9(b) the variant of the ASBM that uses the $(2,2)$ component of the Reynolds stresses, instead of the streamline-normal stress, is shown for additional comparison. The most notable difference is the variability in the length and shape of the recirculation bubble. All models predict bubbles that are longer than that of the LES, with the v^2-f turbulence model predicting the shortest bubble length. As noted in Frohlich et al.,[2] following reattachment, the flow does not fully recover, the skin-friction remains close to zero, and one of the LES sub-grid models does indeed predict a renewed – yet negligible – separated state around $x \approx 7$. These post-reattachment behavior, thus, is not in sharp contrast to the RANS models, which predict separated flow over a long extent.

The LES bubble has a shape that is more round, whereas the separation bubbles obtained with the turbulence models – especially that predicted by the variant of the ASBM – have thinner flattened forms. Along the lines of such behavior, RANS models predict more acute reattachment streamlines than those of the LES, which signifies a slower recovery and hence a delayed re-attachment point. Models based on the ϵ equation tend to predict the separation point further downstream than the LES or the SST model. The point of separation predicted by the LES occurs at $x \approx 0.22$, and that by the SST at $x \approx 0.25$. The v^2-f predicts separation at $x \approx 0.31$, the ASBM at $x \approx 0.33$ and the variant of the ASBM at $x \approx 0.45$.

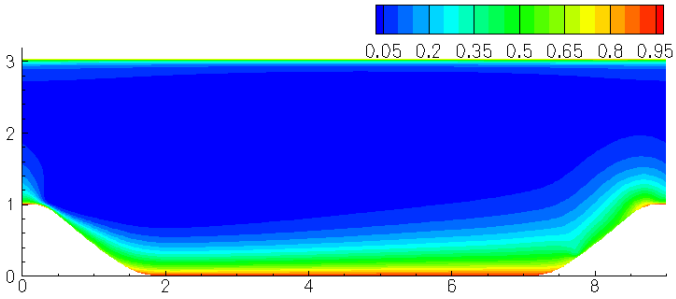

Figure 10. Contours for the wall-blocking tensor component B_{22}.

To give a general sense of the sensitivity of the flow on the wall-blocking effect, Fig. 10 shows the contours for the wall-normal component of the blocking tensor (B_{22}). High values for B_{22} extend farther away from the bottom wall as compared to the upper wall. Unlike the flat periodic channel for which B_{22} is the only non-zero component, non-zero values for B_{11} and B_{22} are also realized.

V.C. Converging-Diverging Channel

The flow through a converging-diverging channel with $Re_\tau \approx 395$[24] and $Re_\tau \approx 617$,[25] for which extensive DNS data is available, was studied next. The corresponding Reynolds numbers based on channel half height δ and maximum inlet velocity U_∞ are approximately 7900 and 12600. Results in this paper are shown for the higher Re case only, since results for the lower Re case are qualitatively similar. The channel geometry, shown in figure 11, consists of a curved, no-slip bottom wall, which has the shape of a bump with a maximum height of approximately 0.67 units, and a flat, no-slip upper wall. The streamwise (x) extent of the domain is 4π and the length in the normal (y) direction is 2. The DNS had a spatial resolution of $N_x = 2304,\ N_y = 385,\ N_z = 576$. The profiles for the inlet boundary used in the DNS were obtained from a precursor DNS at the same Reynolds number. Periodic boundary conditions were specified at the side walls to represent statistically two-dimensional flow. The turbulent boundary layer separates downstream of the peak of the bump on the lower wall due to the sharp adverse pressure gradient and then reattaches a short distance downstream of separation, thus creating a thin separation bubble. Strong coherent structures are reported by Marquillie et al.[24] around the separation region.

The geometry used by the RANS simulation was expanded with an upstream region larger than that in the DNS to ensure the flow at the inlet is not significantly altered by the curvature-induced pressure gradients. A highly orthogonal mesh – especially close to the boundaries – was used to aid better convergence. The y^+ at the bottom wall for the ASBM simulation ranges from 0.09 to 2.0, and has an average value of 0.77. The profiles specified at the inlet were extracted from previous simulations of a flat periodic channel using the corresponding turbulence model employed to simulate the converging-diverging channel. More emphasis was placed on obtaining inlet profiles that matched the friction Reynolds number of the DNS, instead of the

Downloaded by STANFORD UNIVERSITY on March 2, 2016 | http://arc.aiaa.org | DOI: 10.2514/6.2013-2719

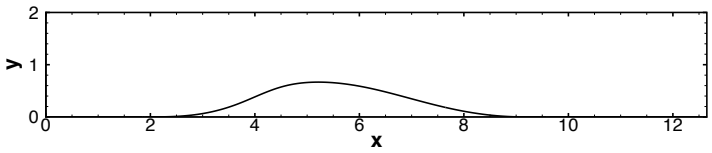

Figure 11. Geometry for the converging-diverging channel.

Reynolds number based on U_∞. As a result, the inlet skin friction is not reproduced exactly. Simulations with slightly varying values of inlet skin-friction, however, showed that the behavior of C_f across the bottom wall, specially around the separation region, is insensitive to the small disagreement at the inlet. The pressure was the only parameter specified at the outlet boundary, and was based on the overall pressure drop of the DNS.

	Separation (x)	Re-attachment (x)	Bubble length
DNS	5.8	6.6	0.8
ASBM	6.4	9.3	2.9
v^2-f	5.8	9.1	3.3
SST	6.0	9.6	3.6

Table 1. Characteristics of the separation bubbles.

The skin-friction and the wall-pressure coefficients are shown in Fig. 12. Good levels of agreement are achieved by the three RANS simulations up to the region slightly before separation. For example, the magnitude of the peak of C_f is well represented by all the models shown. Following separation, the DNS skin-friction experiences a sharp decrease followed by a sharp increase, resulting in a deep, yet brief, separation bubble. This character of the flow makes this case a significant challenge for RANS models. The separation location is best predicted by the v^2-f model, as also shown in Table 1. The ASBM does predict the smallest separation bubble length, shown in Table 1, but this bubble occurs too far downstream, and the depth of the skin-friction is not lower than that of the other models. After reattachment, the DNS profile exhibits a renewed drop in C_f but quickly increases again to its upstream value. This behavior is not reproduced by any of the RANS models.

Satisfactory agreement is observed for the wall-pressure coefficients before reaching the peak of the hump. Following this region, however, the RANS models all equally over-predict the reduction in C_p. The pressure coefficient of the DNS increases after the peak, but its slope shows a sharp decrease over the first half of the separation bubble, and is then followed by a steep increase. The RANS models do not capture such localized behavior, instead, the C_p values increase uniformly from the location of the hump's peak up to the location $x \approx 6.5$. Their slopes then decrease substantially, in disagreement with the DNS.

The contours of the wall blocking tensor component B_{22} are shown in Fig. 13. These figures show that the wall blocking tensor decreases in value over the separated region. A similar decrease in value is also observed at the top wall slightly downstream of the streamwise location of the separated bubble, although the flow does not fully separate in the upper wall.

VI. Conclusion

Structure-based models focus on the componentality, dimensionality, and other properties of the flow to improve modeling fidelity. The dimensionality tensor, which is defined in terms of the non-local fluctuating stream function, provides directional information not contained in the Reynolds stress. The dimensionality tensor, along with other structure tensor such as the circulicity and stropholysis described elsewhere,[4] are used to interpret characteristics of flow structures, such as the near-wall streaks, which play a critical role in turbulent separated flows.

The ASBM focuses on characterizing hypothetical eddies with a single axis of independence. An averaging

Downloaded by STANFORD UNIVERSITY on March 2, 2016 | http://arc.aiaa.org | DOI: 10.2514/6.2013-2719

Downloaded by STANFORD UNIVERSITY on March 2, 2016 | http://arc.aiaa.org | DOI: 10.2514/6.2013-2719

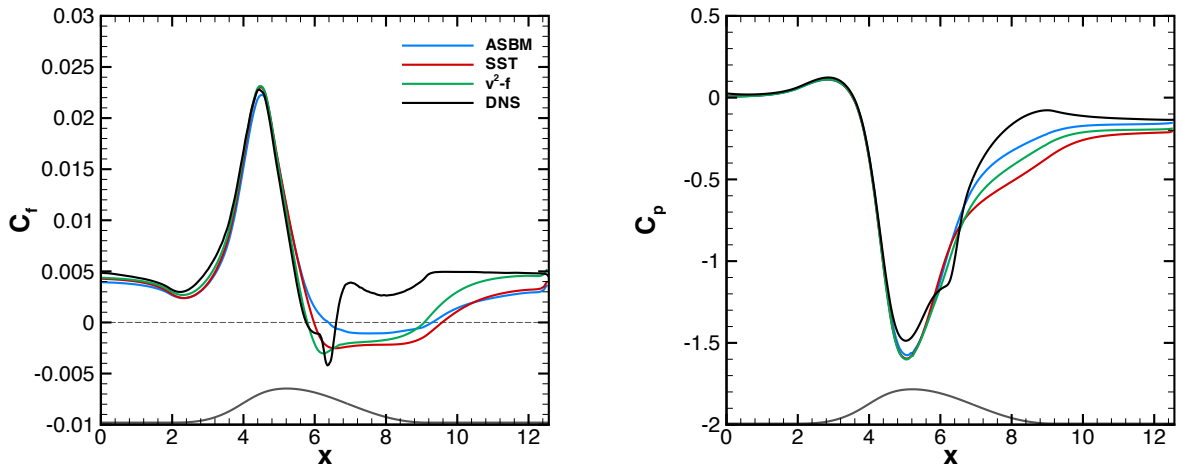

(a) (b)

Figure 12. (a) Skin-friction coefficient $C_f = \tau_w/(0.5\rho U_\infty^2)$, and (b) wall-pressure coefficient $C_p = (p_{wall} - p_{ref})/(0.5\rho U_\infty^2)$. The reference velocity and pressure are evaluated at $(x, y) = (0, 0.5)$

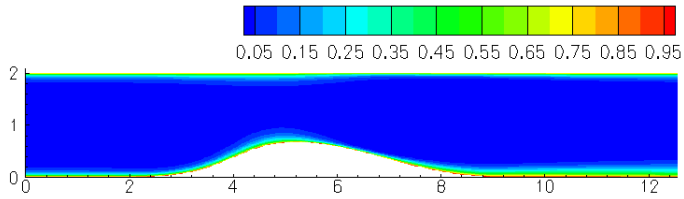

Figure 13. Contours for the wall-blocking tensor component B_{22}.

procedure for such eddies has previously been used to derive expressions for r_{ij} and d_{ij}. Formulations for the parameters of the hypothetical eddies are based on exact solutions of isotropic flow and RDT for a variety of deformations. In this work, we have selected transport equations for k and ϵ to compute the turbulent kinetic energy and turbulence scales at an adequate level of accuracy for use within the ASBM formulation. Additionally, a novel approach that directly realigns the Reynolds stresses instead of the eddy axis tensor has been introduced to account for the inviscid wall-blocking effect encountered near no-slip walls. It is also demonstrated that a strong implicit coupling of the mean flow and turbulence equations is required to achieve converged solutions.

Results show excellent agreement for the periodic channels of Moser, Kim & Mansour[21] and Hoyas & Jimenez.[22] The ASBM was able to reproduce the variability of the normal stresses with a large degree of accuracy. However, results for the massive separation in the periodic hill and the small separation in the converging-diverging channel showed that while the ASBM compares favorably to EVMs, the results are not significantly better. The length of the separation bubble was overpredicted by all models in both the periodic hill and the converging-diverging channel.

The overprediction of separation bubble length could be due to an underprediction of shear stress levels in the separation location and the initial region of the separated shear layer. Another possible cause for the disagreement is the inaccuracy of the overall anisotropy of the stresses that occurs again in the separation location and the initial region of the separated shear layer. Although the ASBM was shown to capture the anisotropy of the stresses upstream of the bubble with a higher level of accuracy, as shown in the flat channel cases, such predictions could be further improved so as to obtain the stronger one-component nature of the flow close to the walls that has been observed in flat channel DNS. Efforts are currently underway to understand the anisotropic behavior of the ASBM using the barycentric maps of Banerjee et al.[26] Ultimately,

regions of parameter space in which the ASBM formulation produces notable discrepancies will be identified, following which the full structure-based model formulation will be employed to provide model refinement.

Acknowledgment

This work was supported by NASA under the grant "Structure Based Modeling for Turbulent Separated Flows". The authors thank the technical monitor Dr. Stephen Woodruff for his collaboration and comments on this work.

References

[1]Bentaleb, Y., Lardeau, S., and Leschziner, M. A., "Large-eddy simulation of turbulent boundary layer separation from a rounded step," *Journal of Turbulence*, Vol. 13, No. 4, 2012, pp. 1–28.

[2]Fröhlich, J., Mellen, C. P., Rodi, W., Temmerman, L., and Leschziner, M. A., "Highly resolved large-eddy simulation of separated flow in a channel with streamwise periodic constrictions," *Journal of Fluid Mechanics*, Vol. 526, March 2005, pp. 19–66.

[3]Kassinos, S. C. and Reynolds, W. C., *A Structure-Based Model for the Rapid Distortion of Homogeneous Turbulence*, Ph.D. thesis, Stanford University, 1995.

[4]Kassinos, S. C., Reynolds, W. C., and Rogers, M. M., "One-point turbulence structure tensors," *Journal of Fluid Mechanics*, Vol. 428, Feb. 2001, pp. 213–248.

[5]Haire, S. L., *Towards an Affordable Two-Equation Structure-Based Turbulence Model*, Ph.D. thesis, Stanford University, 2003.

[6]Langer, C. A. and Reynolds, W. C., *A New Algebraic Structure-Based Turbulence Model for Rotating Wall-Bounded Flows*, Ph.D. thesis, Stanford University, 2003.

[7]Kassinos, S., Langer, C., Kalitzin, G., and Iaccarino, G., "A simplified structure-based model using standard turbulence scale equations: computation of rotating wall-bounded flows," *International Journal of Heat and Fluid Flow*, Vol. 27, No. 4, Aug. 2006, pp. 653–660.

[8]Durbin, P. A., "Separated Flow Comutations with the k eps v2 Model," *AIAA Journal*, Vol. 33, No. 4, 1995, pp. 659–664.

[9]Radhakrishnan, H., Pecnik, R., Iaccarino, G., and Kassinos, S., "Computation of separated turbulent flows using the ASBM model," *Center for Turbulence Research: Proceedings of the Summer Program*, 2008, pp. 365–376.

[10]Pecnik, R., O'Sullivan, J. P., Panagiotou, K., Radhakrishnan, H., Kassinos, S., Duraisamy, K., and Iaccarino, G., "Towards an Accurate and Robust Algebraic Structure Based Model," *Center for Turbulence Research: Proceedings of the Summer Program*, 2012, pp. 283–293.

[11]Bhattacharya, A., Kassinos, S. C., and Moser, R. D., "Representing anisotropy of two-point second-order turbulence velocity correlations using structure tensors," *Physics of Fluids*, Vol. 20, No. 10, 2008, pp. 101502.

[12]Mansour, N. N., Shih, T.-H., and Reynolds, W. C., "The effects of rotation on initially anisotropic homogeneous flows," *Physics of Fluids*, Vol. 3, No. 10, 1991, pp. 2421–2425.

[13]Kida, S. and Hunt, J. C. R., "Interaction between different scales of turbulence over short times," *Journal of Fluid Mechanics*, Vol. 201, 1989, pp. 411–445.

[14]Cambon, C., Jacquin, L., and Lubrano, J. L., "Toward a new Reynolds stress model for rotating turbulent flows," *Physics of Fluids*, Vol. 4, No. 4, 1992, pp. 812–824.

[15]Durbin, P. A., "Near-Wall Turbulence Closure Modeling Without "Damping Functions"," *Theoretical and Computational Fluid Dynamics*, Vol. 3, 1991, pp. 1–13.

[16]Lien, F. S., Kalitzin, G., and Durbin, P. A., "RANS modeling for compressible and transitional flows," *Center for Turbulence Research: Proceedings of the Summer Program*, 1998, pp. 267–286.

[17]Reynolds, W. C., Kassinos, S. C., Langer, C. A., and Haire, S., "New directions in turbulence modeling," *3rd International Symposium on Turbulence, Heat, and Mass Transfer*, 2000.

[18]Pecnik, R., Terrapon, V., Ham, F., and Iaccarino, G., "Full system scramjet simulation," *Center for Turbulence Research: Proceedings of the Summer Program*, 2009, pp. 33–45.

[19]Palacios, F. and Alonso, J. J., "New convergence acceleration techniques in the Joe code," *Center for Turbulence Research: Proceedings of the Summer Program*, 2011, pp. 297–308.

[20]Balay, S., Brown, J., Buschelman, K., Gropp, W. D., Kaushik, D., Knepley, M. G., McInnes, L. C., Smith, B. F., and Zhang, H., "PETSc Web page," 2013, http://www.mcs.anl.gov/petsc.

[21]Moser, R. D., Kim, J., and Mansour, N. N., "Direct numerical simulation of turbulent channel flow up to Reτ=590," *Physics of Fluids*, Vol. 11, No. 4, 1999, pp. 943–945.

[22]Hoyas, S. and Jimenez, J., "Scaling of the velocity fluctuations in turbulent channels up to Reτ=2003," *Physics of Fluids*, Vol. 18, No. 1, 2006, pp. 011702.

[23]Jang, Y. J., Leschziner, M. A., Abe, K., and Temmerman, L., "Investigation of Anisotropy-Resolving Turbulence Models by Reference to Highly-Resolved LES Data for Separated Flow," *Flow, Turbulence and Combustion*, Vol. 69, 2003, pp. 161–203.

[24]Marquillie, M., Laval, J.-P., and Dolganov, R., "Direct numerical simulation of a separated channel flow with a smooth profile," *Journal of Turbulence*, Vol. 9, No. 1, 2008, pp. 1–23.

[25]Marquillie, M., Ehrenstein, U., and Laval, J.-P., "Instability of streaks in wall turbulence with adverse pressure gradient," *Journal of Fluid Mechanics*, Vol. 681, No. 2011, June 2011, pp. 205–240.

Downloaded by STANFORD UNIVERSITY on March 2, 2016 | http://arc.aiaa.org | DOI: 10.2514/6.2013-2719

[26]Banerjee, S., Krahl, R., Durst, F., and Zenger, C., "Presentation of anisotropy properties of turbulence, invariants versus eigenvalue approaches," *Journal of Turbulence*, Vol. 8, No. 32, Jan. 2007.

Downloaded by STANFORD UNIVERSITY on March 2, 2016 | http://arc.aiaa.org | DOI: 10.2514/6.2013-2719